TU Delft

Delft University of Technology

Document Version
Final published version

Licence
CC BY

Citation (APA)
Plumaris, M., Thai, T., Rovera, D., Iess, L., Dirkx, D., & Sesia, I. (2026). Passive TWSTFT: a cost-effective alternative for robust UTC(k) dissemination. *Metrologia*, *63*(4). https://doi.org/10.1088/1681-7575/ae9310

Important note
To cite this publication, please use the final published version (if applicable).
Please check the document version above.

Copyright
In case the licence states “Dutch Copyright Act (Article 25fa)”, this publication was made available Green Open Access via the TU Delft Institutional Repository pursuant to Dutch Copyright Act (Article 25fa, the Taverne amendment). This provision does not affect copyright ownership.
Unless copyright is transferred by contract or statute, it remains with the copyright holder.

Sharing and reuse
Other than for strictly personal use, it is not permitted to download, forward or distribute the text or part of it, without the consent of the author(s) and/or copyright holder(s), unless the work is under an open content license such as Creative Commons.

Takedown policy
Please contact us and provide details if you believe this document breaches copyrights.
We will remove access to the work immediately and investigate your claim.

This work is downloaded from Delft University of Technology.

PAPER • OPEN ACCESS

Passive TWSTFT: a cost-effective alternative for robust UTC(k) dissemination

To cite this article: Michael Plumaris *et al* 2026 *Metrologia* **63** 045005

View the article online for updates and enhancements.

You may also like

- Time transfer with nanosecond accuracy for the realization of International Atomic Time
D Piester, A Bauch, L Breakiron et al.
- Use of software-defined radio receivers in two-way satellite time and frequency transfers for UTC computation
Zhiheng Jiang, Victor Zhang, Yi-Jiun Huang et al.
- Stability improvement of an operational two-way satellite time and frequency transfer system
Yi-Jiun Huang, Miho Fujieda, Hiroshi Takiguchi et al.

This content was downloaded from IP address 131.180.130.25 on 18/08/2026 at 13:56

Metrologia



Check for updates

OPEN ACCESS

RECEIVED
9 April 2026

REVISED
30 July 2026

ACCEPTED FOR PUBLICATION
31 July 2026

PUBLISHED
12 August 2026

Original content from this work may be used under the terms of the Creative Commons Attribution 4.0 licence.

Any further distribution of this work must maintain attribution to the author(s) and the title of the work, journal citation and DOI.



PAPER

Passive TWSTFT: a cost-effective alternative for robust UTC(k) dissemination

Michael Plumaris[1,*], Tung Thai[2], Daniele Rovera[3], Luciano Iess[4], Dominic Dirkx[5] and Ilaria Sesia[2]

[1] European Space Agency, Noordwijk, The Netherlands
[2] Istituto Nazionale di Ricerca Metrologica, Turin, Italy
[3] Time and Frequency Solution (TFSol), Aix-en-Provence, France
[4] Department of Mechanical and Aerospace Engineering, Sapienza University of Rome, Rome, Italy
[5] Delft University of Technology, Delft, The Netherlands
[*] Author to whom any correspondence should be addressed.

E-mail: michael.plumaris@esa.int

Keywords: time transfer, two-way satellite time and frequency transfer, orbit determination, satellite delay calibration, software-defined radio, UTC dissemination

Abstract

Two-way satellite time and frequency transfer (TWSTFT) is among the most accurate techniques for comparing clocks over (inter)continental baselines, exchanging bidirectional signals through a geostationary satellite—but the cost and complexity of an active (Tx & Rx) terminal restrict it to a handful of Coordinated Universal Time (UTC)(k) laboratories. We show that a passive, receive-only user can reach those same laboratories by reducing a one-way pseudorange for the satellite-motion, atmospheric, and equipment delays. Using active-network observations over 130 d, the satellite ephemeris is reconstructed by orbit determination (OD). A portable terminal—a commercial TV dish and a software-defined-radio receiver—was calibrated in common-clock mode at INRiM and deployed to the Côte d"Azur Observatory (OCA). Over a 40 d campaign, time transfer to three UTC(k) laboratories agreed with independent GNSS and active-TWSTFT links at the nanosecond level; despite larger short-term noise from solar-radiation-pressure and wet-tropospheric mismodelling, the overlapping Allan deviation reaches $\approx 10^{-14}$ at one day, matching GNSS performance. The accuracy is bounded by an ≈ 7 ns (1σ) budget, and an INRiM–OCA–INRiM closure sequence confirmed robustness to relocation and traceability to UTC(k). Passive TWSTFT thus offers a scalable, interference-resilient, and low-cost route to UTC(k) dissemination, with future work targeting automated OD for quasi-real-time operation.

1. Introduction

Two-way satellite time and frequency transfer (TWSTFT) [1, 2], also referred to as TW, has played an instrumental role in global timekeeping, serving as a primary technique for the computation of International Atomic Time and the derived Coordinated Universal Time (UTC). Its operational use and data exchange procedures are governed by ITU Recommendation TF.1153 [3]. Owing to its reciprocal measurement principle, TW currently achieves a statistical uncertainty of approximately 1 ns.

TW operates through the simultaneous bidirectional exchange of radiometric signals between two stations connected via a geostationary satellite acting as a transparent telecommunications relay. The transmitted signals embed pseudorandom noise (PN) codes phase-modulated by the local clock"s one-pulse-per-second (1PPS) signal. By correlating the incoming signal with a locally generated PN replica, the receiver reconstructs the remote 1PPS and compares it against its local clock reference. Differencing the exchanged datasets yields the inter-station clock offset. The reciprocal TW geometry cancels common-mode path delays (satellite motion, atmosphere)

© 2026 The Author(s). Published on behalf of BIPM by IOP Publishing Ltd

and the non-reciprocal effects in the station hardware are calibrated periodically[6] to maintain long-term accuracy.

A key limitation of conventional TW is that participation is restricted to active users transmitting signals through the satellite transponder. This constraint limits scalability due to the rigid operational scheme and the finite bandwidth available on the communication satellite. Moreover, the specialised infrastructure required—including dedicated satellite transponder capacity and calibrated ground stations—results in operational costs significantly higher than those associated with GNSS time transfer techniques.

To overcome this limitation, a 'passive' TW configuration is proposed: a receive-only user synchronises to UTC(k) by relying on orbit determination (OD) of the satellite to characterise the end-to-end signal delays. Proof-of-concept demonstrations using the active TW network have been reported by Rieck *et al* [4] and within the European DEMETRA project [5]. The present work targets the end-to-end implementation of passive TW, including system conceptualisation, field experimentation, and performance validation. The remainder of this paper is organised as follows. Section 2 describes the methodology and experimental setup. Section 3 presents the OD strategy and delay modelling approach. Section 4 reports the experimental results, and the final section summarises the conclusions and outlines future work.

2. Methodology

The passive TW methodology comprises two interconnected components: satellite OD and the deployment of a passive user terminal. This section first reviews the active TW observables, then introduces the one-way pseudorange exploited by a passive user, and discusses the resulting modelling challenges and the user calibration.

Figure 1 illustrates the radiometric observables exchanged within the active TW network, whose geographical distribution across European and U.S. UTC(k) laboratories is shown in figure 2. The network operates according to a coordinated bi-hourly schedule of successive measurement sessions, each consisting of a 60 s configuration phase followed by a 120 s measurement phase.

Within each schedule cycle two observable types are acquired sequentially: a ranging measurement (ρ_{kk}) where the station recovers its own signal relayed by the satellite, and reciprocal pseudorange exchanges (ρ_{kj}) with the other stations. In each session the recovered remote 1PPS is compared against the local clock by a time-interval counter (TIC), which measures their difference TI(k); the 1 s raw data collected over the session are reduced to a single value through a quadratic fit, designated TW(k). The clock difference between two active stations k and j is then formed from the linear combination [3]

$$\Delta\tau_{kj} = \frac{1}{2}\left[\mathrm{TW}\,(k) - \mathrm{TW}\,(j)\right] + \frac{1}{2}\left(\Delta_{\mathrm{sat}} + \Delta_{\mathrm{Sag}} + \Delta_{\mathrm{atmo}} + \Delta_{(\mathrm{Tx-Rx})}\right)_{kj} \quad (1)$$

where the second term collects the delays that are (mostly) reciprocal and therefore largely cancel out: the satellite transponder (Δ_{sat}), the Sagnac effect (Δ_{Sag}), the atmospheric delays (Δ_{atmo}). The transmit-receive delays ($\Delta_{(\mathrm{Tx-Rx})}$) are monitored via calibrations using mobile equipment.

In this work the OD filter processes the *individual* pseudorange observables, modelled as

$$\rho_{kj} = \frac{R_{kj}}{c} + \Delta\tau_{kj} + \mathrm{Tx}_k + \mathrm{Rx}_j + d_{\mathrm{sat}} + d_{\mathrm{atmo},kj} \quad (2)$$

where R_{kj} is the geometric slant range via the satellite, $\mathrm{Tx}_k + \mathrm{Rx}_j$ the composite transmit and receive delays of the two stations, and d_{sat}, $d_{\mathrm{atmo},kj}$ the transponder and atmospheric delays. Unlike the TW combination of equation (1), none of these cancel by reciprocity: the slant range R_{kj} (via the OD ephemeris) and the atmospheric delay $d_{\mathrm{atmo},kj}$ are modelled explicitly, whereas the station delays $\mathrm{Tx}_k + \mathrm{Rx}_j$ are lumped into a single constant per-link bias estimated in the OD.

Both observable types contribute to the orbit estimation. In the nominal schedule each station acquires a ranging observation (ρ_{kk}) every one to two hours and a reciprocal pseudorange (ρ_{kj}) with each partner station every two hours; the pseudoranges therefore dominate in number ($\approx 80\%$) and, spanning many station baselines, provide the geometric diversity in the slant range R_{kj} that constrains the satellite state. For the ranging observables, the composite station delay can be measured locally: in this experiment the delay $\mathrm{Tx}_{\mathrm{IT01}} + \mathrm{Rx}_{\mathrm{IT01}}$ was measured through a dedicated calibration loop[7] and fixed in the OD, anchoring the orbit along the IT01–satellite line of sight. Even so, the remaining station delays are difficult to decorrelate given the quasi-stationary dynamics and narrow observation geometry.

The transponder group delay d_{sat} is obtained from the manufacturer specifications [6]; for the transatlantic links it combines the delays of the two channels traversed, and it cannot be reliably separated from the station delays in the OD. Atmospheric delays are modelled as described in

[6] Typically performed on a two-year cycle; see https://webtai.bipm.org/ftp/pub/tai/publication/twstft-calibration/.

[7] A satellite simulator was implemented by placing a frequency downconverter, with negligible delay, at the antenna reference point, allowing the global station delay $\mathrm{Tx}_{\mathrm{IT01}} + \mathrm{Rx}_{\mathrm{IT01}}$ to be measured directly by the TW modem.

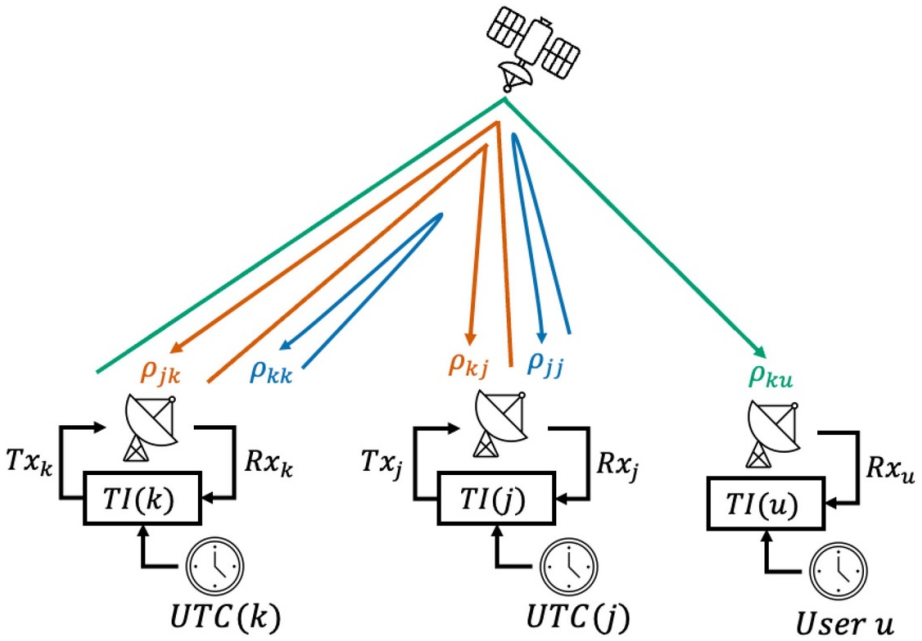


Figure 1. Radiometric observables in the active TW network and passive user configuration. Active stations k and j exchange signals via a geostationary satellite to form ranging (ρ_{kk}) and pseudorange (ρ_{kj}) observables, from which the clock difference $\Delta\tau_{kj}$ is derived. A passive user u records the one-way signal ρ_{ku}; after correcting for geometric range, propagation delays, satellite transponder delay, and calibrated $\mathrm{Tx}_k + \mathrm{Rx}_u$ station delays, the user clock can be synchronised to the corresponding UTC(k).

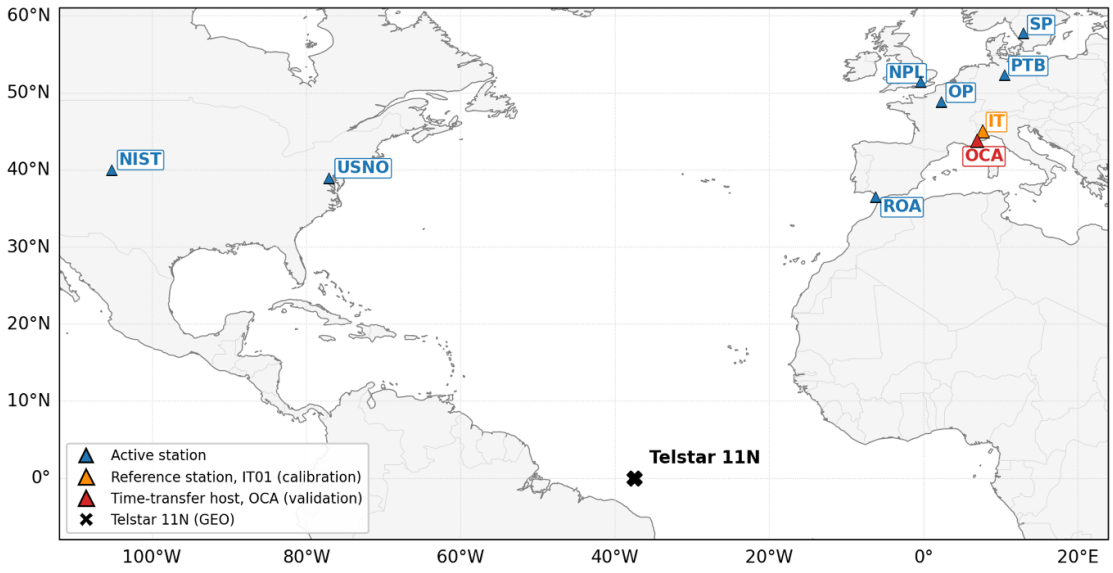


Figure 2. UTC(k) laboratories of the active TW network considered in this work. IT01 (orange) is the reference station at the Italian Metrology Institute (INRiM) in Turin, whose internal delays were measured for calibration; the Côte d"Azur Observatory (OCA, Calern; red) is the passive-user time transfer host used for the experimental validation (section 4).

section 3.3. Antenna-position uncertainties induce attitude-dependent range errors, since the satellite phase centre is not precisely known relative to the centre of mass.

Prior to remote deployment, the passive user u is co-located with a reference active station in a common-clock configuration, enabling calibration of the composite delay $\mathrm{Tx}_k + \mathrm{Rx}_u$, as detailed in section 4.2. After deployment, the passive user operates in receive-only mode to measure its local clock against the broadcast signal from active station k (ρ_{ku}). This measurement equation can be rewritten as

$$\Delta\tau_{uk} = \rho_{ku} - \frac{\widehat{R}_{ku}}{c} - d_{\mathrm{atmo},ku} - d_{\mathrm{sat}} - (\mathrm{Tx}_k + \mathrm{Rx}_u) \tag{3}$$

where $\widehat{R}_{ku}$ is obtained by interpolating the satellite ephemeris. This formulation enables direct synchronisation of the passive user clock to the corresponding UTC(k) realisation.

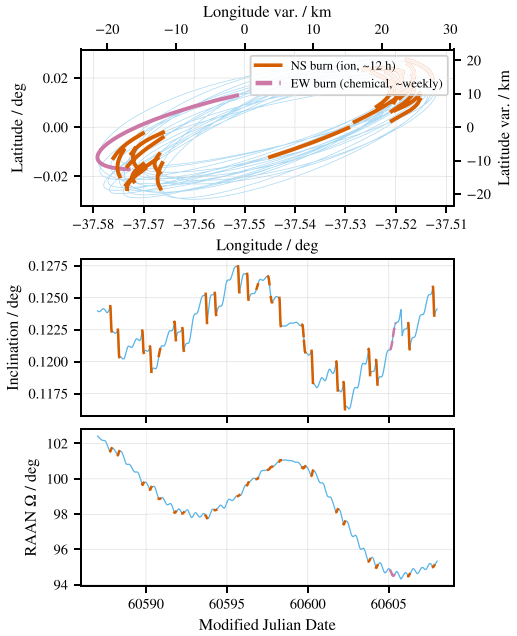


Figure 3. Telstar 11 N latitude–longitude flight envelope about the 37.55° W slot; *middle:* osculating inclination; *bottom:* right ascension of the ascending node (RAAN, unwrapped).

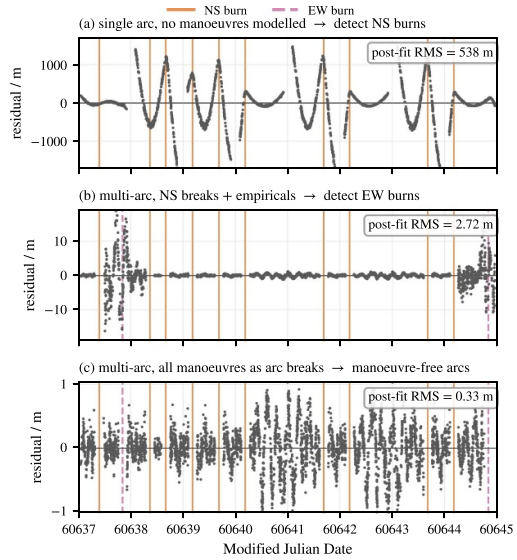


Figure 4. Iterative manoeuvre detection. Post-fit ranging residuals reduce across *(a)* no manoeuvres modelled; *(b)* NSSK identified, exposing the weaker EWSK burns; *(c)* all manoeuvres bounded.

3. Orbit determination

The fundamental pillars of OD are high-fidelity dynamical and observation models. Starting from an initial guess[8], the dynamical model captures all relevant accelerations to accurately propagate the satellite position over time, yielding a reference trajectory. Using ground-station coordinates and signal time-of-flight corrections, the observation model generates simulated observables. A batch least-squares filter iteratively adjusts the estimated parameters to minimise the residuals between simulated and measured observables until convergence is achieved. The OD is performed with the open-source *Tudat* astrodynamics software toolbox [7, 8].

3.1. Dynamical model

Telstar 11 N is a geostationary communication satellite relaying TW operations across the European and transatlantic networks. Driven by perturbing accelerations, it oscillates daily about its nominal slot (figure 3), so that the satellite–user range changes at $\approx$0.5 m s^{-1} on average. The dominant perturbation is third-body attraction from the Sun and Moon ($\approx 10^{-5}$ m s^{-2}), which together with Earth's oblateness precesses the orbital plane and drives the daily latitude oscillation, while Earth's triaxiality induces a slow longitudinal drift.

Solar radiation pressure (SRP) represents a major source of uncertainty for geostationary satellites due to the poorly constrained reflectance properties of large solar arrays. This perturbation modulates the orbital eccentricity, affecting both orbital radius and longitude. In the absence of spacecraft attitude telemetry, the spacecraft is represented by a panel-based macro-model with a nadir-pointing bus and Sun-pointing arrays; mass-scaling and reflectance coefficients are estimated as solve-for parameters, and residual mismodelling is absorbed by empirical accelerations in the radial, along-track, and cross-track directions.

3.2. Station-keeping manoeuvres

To remain within its assigned slot, a geostationary satellite must periodically counteract the perturbing forces through orbit-maintenance manoeuvres. These divide into north–south station keeping (NSSK), which controls the orbital inclination and dominates the annual Δv budget, and east–west station keeping (EWSK), which corrects the longitudinal drift and eccentricity. Geostationary platforms have historically used chemical thrusters (bipropellant hydrazine) for both, with typically one to two burns per month [9]. Newer platforms increasingly adopt ion (electric) propulsion, trading the operational convenience of the brief, infrequent high-precision chemical burns for substantial fuel-mass savings over a 15-year-plus mission. Telstar 11 N adopts a hybrid architecture [10]: ion thrusters perform NSSK and chemical thrusters the EWSK. The operator does not disclose the manoeuvre epochs, so they occur unpredictably, disrupting the dynamical continuity in the OD solution.

A multi-arc strategy is therefore adopted: the satellite state is estimated independently on each

[8] Obtained by propagating SGP4 two-line elements retrieved from Celestrak, https://celestrak.org.

arc, with the arcs delimited by the manoeuvre epochs. These are identified by a sequential detection algorithm that inspects the post-fit residuals, illustrated in figure 4. An initial single-arc OD with no manoeuvres modelled yields residuals of order 10^2 m (panel (a)); the NSSK events are located from second-derivative discontinuities in these residuals, appearing as near-daily alternating north–south firings about 12 h apart. Re-estimating the state on the resulting arcs, while absorbing residual mismodelling with ad hoc empirical accelerations, reveals the EWSK burns (panel (b)). These are harder to locate—they act along the poorly observed along-track direction and leave only a weak residual signature—but once found they too become arc boundaries, yielding manoeuvre-free arcs whose residuals settle at the metre level (panel (c)).

The manoeuvres are bypassed in this way rather than estimated because neither class can be solved for reliably. The NSSK firings are extended, low-thrust ion burns of unknown duration and pointing; recovering their finite-duration thrust profile is ill-posed without propulsion telemetry. The EWSK burns are near-impulsive and thus better suited to a solve-for Δv, yet the operator"s real-time attitude adjustments vary the thrust direction from burn to burn, so the recovered impulses did not generalise and the residuals remained unsatisfactory for TW applications. More effective manoeuvre mitigation—for realtime capability—is the subject of ongoing work.

3.3. Time-of-flight corrections

Modelling the pseudorange requires correcting the signal time of flight for atmospheric and relativistic effects, applied within an iterative time-of-flight solution that evaluates the satellite state at the transmission, reflection, and reception epochs[9].

The dominant correction is tropospheric (figure 5, top) modelled with the Vienna Mapping Function 3 (VMF3) [11], which supplies site-specific hydrostatic and wet zenith delays and mapping functions ray-traced from numerical weather models [12]. The hydrostatic part is accurate to the millimetre, whereas the wet part—driven by water-vapour variability—reaches the 20 cm level in the zenith [13] and dominates the error budget. A co-located GNSS receiver could help evaluate this term, although the low elevation of the geostationary satellite (∼20°–30°) inflates the mapping function and limits the achievable gain.

[9] See https://py.api.tudat.space/en/latest/estimation/observable_models_setup/light_time_corrections.html for details on the model.

The dispersive ionospheric delay (figure 5, bottom) is

$$d_{\text{iono}} = \frac{40.3}{c}\left(\frac{\text{STEC}_{\text{down}}}{f_{\text{down}}^2} + \frac{\text{STEC}_{\text{up}}}{f_{\text{up}}^2}\right), \qquad (4)$$

where STEC are the slant total electron content on the up- and down-leg. Each is obtained from the Jakowski *et al* [14] analytical vertical-TEC (VTEC) model with a modified single-layer mapping function: the VTEC at the sub-ionospheric point is computed as a function of geomagnetic latitude, local time, and solar activity, and mapped to the slant geometry through $\text{STEC} = \text{VTEC}/\cos z'$, with z' the zenith angle at the ionospheric pierce point.

The Sagnac effect, arising from Earth's rotation, produces an apparent delay—positive toward the east—that can reach 100 ns−200 ns for intercontinental baselines. Since the orbit is propagated in an inertial frame, this delay is naturally accounted for when transforming to the Earth-fixed frame.

Finally, the gravitational (Shapiro) delay is evaluated in the geocentric frame with the receiver proper time as the observable. The Sun's monopole contribution—∼5 ns in barycentric coordinates—is almost entirely reabsorbed into the time-scale transformation to the geocentric frame [15], leaving only a negligible tidal part ($\sim 10^{-16}$ s); the retained Earth monopole term,

$$\Delta_{\text{Shapiro}} = \frac{2\text{GM}_\oplus}{c^3}\ln\left(\frac{r_{\text{sat}} + r_{\text{gs}} + r_{\text{sat-gs}}}{r_{\text{sat}} + r_{\text{gs}} - r_{\text{sat-gs}}}\right), \qquad (5)$$

amounts to ≈ 135 ps for pseudoranges ρ_{kj}, which matches twice the value calculated for GNSS downlink-only signals [16].

3.4. Residual analysis

The OD filter uses a batch least-squares approach to process the active-network TW observations over 130 d, partitioned into 153 manoeuvre-bounded arcs. Set by the station-keeping cadence, the arc durations vary significantly, from 4 h to 4.5 d. This creates a split between *local* parameters—the per-arc initial state, and piecewise-constant RSW empirical accelerations—and *global* parameters—the composite Tx+Rx delay of each link, held fixed only on the measured IT01–IT01 loop. Observables are weighted according to measurement noise, represented by the RMS residual of the quadratic fit applied to the TIC 1PPS measurements.

The post-fit residuals (figure 6) show no long-term trend; their RMS is 0.18 m–0.24 m depending on the link configuration. A clear diurnal modulation remains, which we ascribe to the daily attitude reorientation and the phase-centre and SRP variations it induces, only partly absorbed by the RSW empirical accelerations. These (fourth panel) are comparable

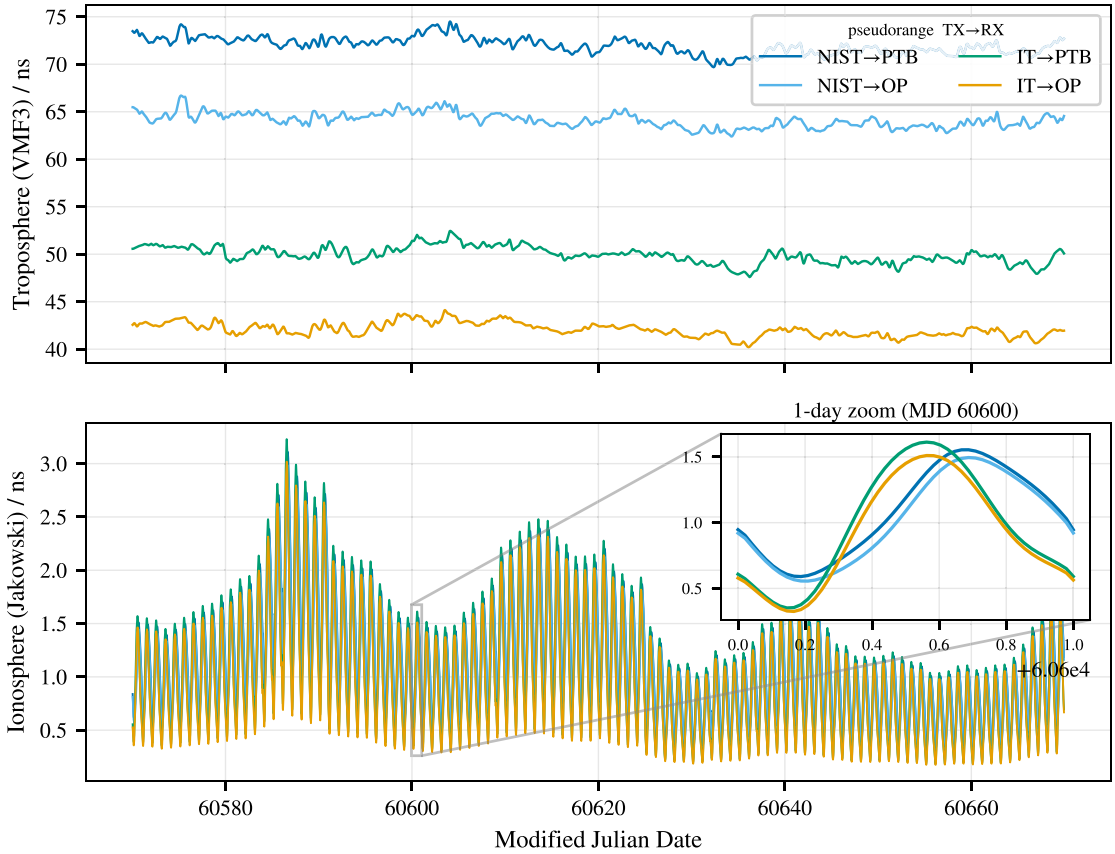


Figure 5. Simulated atmospheric corrections for a representative set of TW links: tropospheric delay (top) and ionospheric delay (bottom). Earth-induced Shapiro is not shown, as it is constant across all links.

across the three axes ($\sim 5 \times 10^{-7}$ m s^{-2}), so no single direction carries an unmodelled signature.

The slightly larger EU pseudorange residuals before MJD 60 583 are associated with the active-network calibration values update. In the TW time transfer products this introduces link steps, but the impact on the OD pseudorange is reduced, leaving only a residual at the $\sim$1 ns level. The pre-MJD-60 583 data are *retained*, since they carry the pre-trip user calibration (table 1).

The estimation geometry shapes these uncertainties. Lower-latitude stations, seen at higher elevation, sharpen observability, and the transatlantic (NIST, USNO) links are essential for capturing the longitudinal dynamics.

The per-arc state is best determined radially ($1\sigma \approx 1$ m–3 m), an order of magnitude tighter than the along- and cross-track components (tens of metres), as expected for ranging to a geostationary target. Every ground user views the satellite within the $\approx 8.7^\circ$ Earth-limb cone about nadir, so the line of sight is nearly radial and the large transverse state errors enter only through their small off-nadir projection ($\sin\theta \lesssim 0.15$); the user range error is thereby held to the few-metre (nanosecond) level across the network.

The composite link delays are strongly correlated ($\rho \gtrsim 0.8$) through the fixed IT01 reference, so the OD constrains the *differences* between link delays far better than their absolute values. Because the time transfer products are themselves differential (UTC(k)−UTC(j)), this shared common-mode uncertainty cancels and does not limit the result. Their formal uncertainty splits geographically and grows as the user moves away from the IT01 reference station, and can be reduced by additional loop calibrations in the active TW network.

To evaluate the robustness of the estimated station delays, figure 7 compares clock offsets derived from active and passive TW solutions. The active TW solution employs equation (1) using the calibrated differential $\Delta_{(\mathrm{Tx-Rx})}$ delays, whereas the passive solution relies on equation (2) with the individual Tx + Rx composite delays estimated directly by the OD filter. Both approaches agree to an RMS of approximately 0.8 ns, over 30 links, confirming that the OD provides a reliable basis for subsequent calibration and traceability analysis. This comparison also sets the 4 h empirical-acceleration interval: finer grids overfit (the radial accelerations absorb station-delay signatures, opening an active–passive offset), while coarser grids leave excess dynamical mismodelling in the ephemeris. In the presence of anomalies or outages affecting one end of an active TW link, these results demonstrate the feasibility of reconstructing

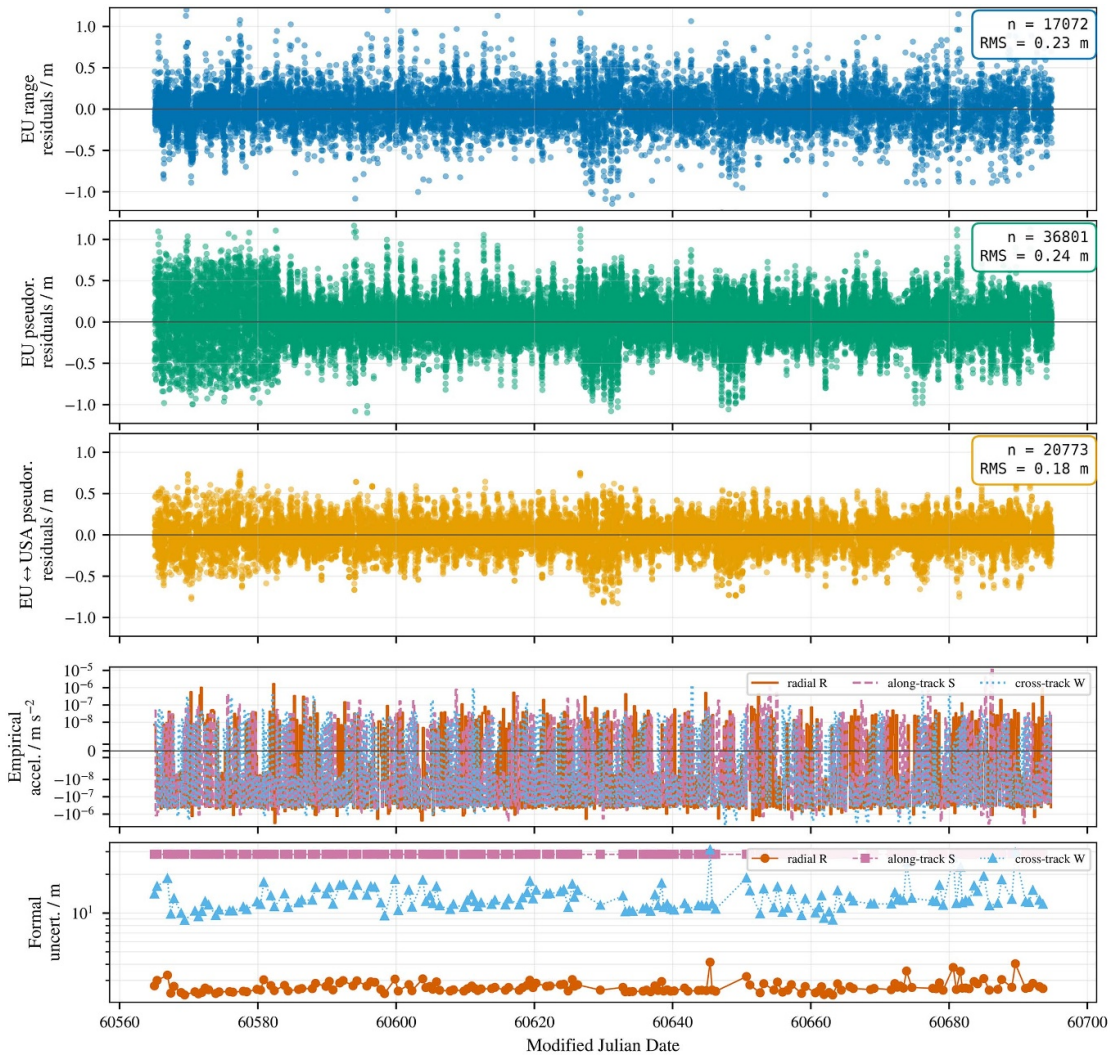


Figure 6. Orbit-determination diagnostics for the multi-arc solution. *Top three panels:* post-fit one-way residuals grouped by observable type: intra-European ranging, intra-European pseudoranging, and Europe–US pseudoranging. *Fourth panel:* estimated RSW empirical accelerations, restarted at every arc boundary. *Bottom panel:* the per-arc initial-state position formal uncertainty (1σ) in the RSW frame, from the regularised posterior covariance—radial the best determined, along-/cross-track an order of magnitude weaker.

UTC(k) clock differences using one-way pseudorange measurements.

4. Experimental phase

Having established the feasibility of determining the satellite ephemeris, the next objective is to evaluate the passive TW system under operational conditions. The experimental phase is designed to assess its performance in terms of accuracy, stability, and practical deployment considerations.

4.1. Passive user setup

The portable passive user terminal, schematised in figure 8, is designed to acquire and process pseudoranging signals for synchronisation with UTC(k). Signal reception is performed using a 100 cm Ku-band dish antenna commonly employed for satellite television applications, coupled to a low-noise block (LNB) downconverter operating with a 9.75 GHz local oscillator. The LNB amplifies the received signal and downconverts it to the L-band. The resulting signal is subsequently processed by a dedicated downconverter to produce a 70 MHz intermediate frequency, which is sampled and digitised by an analogue-to-digital converter.

The digitised signal is processed by a software-defined radio (SDR) receiver that performs PN-code demodulation and recovers the 1PPS signal. Compared with conventional analogue TW modems, the SDR implementation provides enhanced flexibility, digital filtering capability, and improved resilience to interference and multipath effects [17], while enabling simplified signal acquisition and cost-effective portable deployment.

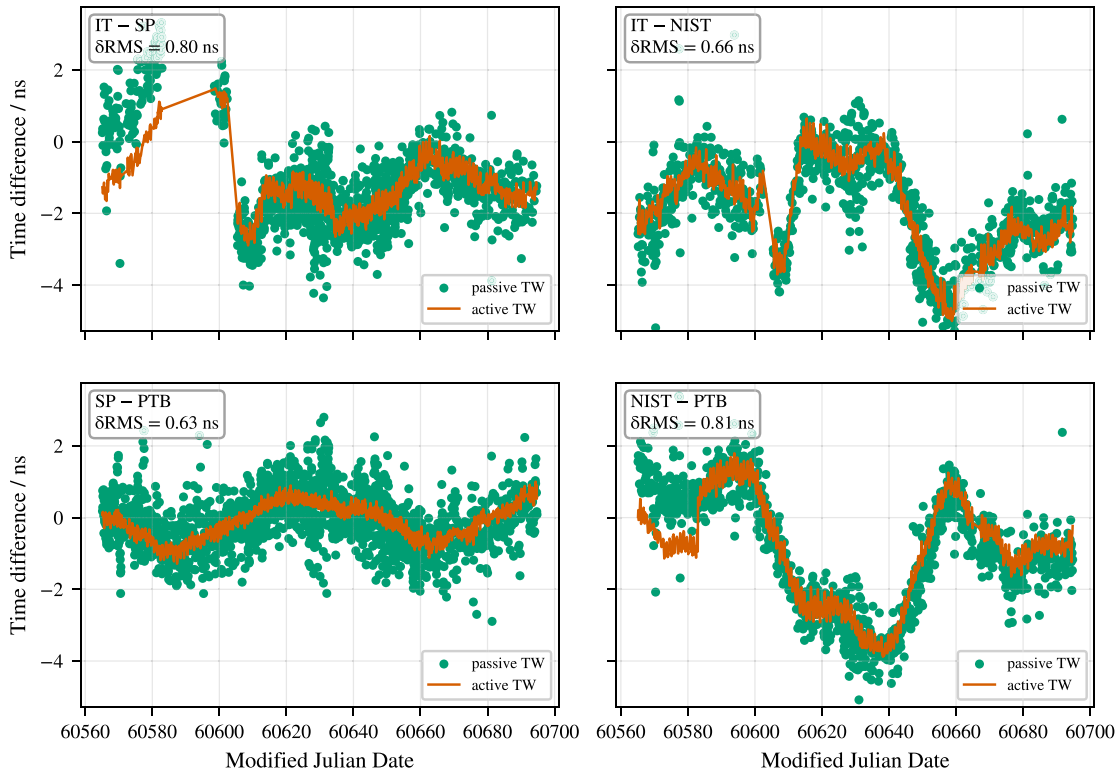


Figure 7. Active versus passive TW clock differences UTC(a)−UTC(b) for four station baselines. Each panel is annotated with the agreement δRMS, which stays at the $\lesssim$1 ns level, consistent with the OD post-fit residuals. The step near MJD 60 583 in IT−SP and NIST−PTB is the active-network calibration update; the passive solution, a geometric estimate with a single bias per link, is continuous across it.

The 10 MHz reference signal generated by the user clock is used to synchronise the sampling rate of the digitiser and to generate the 1PPS signal that serves as the reference point for measuring the delay between the local time scale and the internal time base of the SDR.

4.2. Calibration at INRiM

The calibration procedure aims to determine the composite delay between the transmitting station and the passive user terminal, which is required to establish traceability to UTC(k) and, by extension, to UTC. The passive TW terminal was calibrated at INRiM by adopting UTC(IT) as the user clock, thereby operating in a common-clock configuration with the local active TW station.

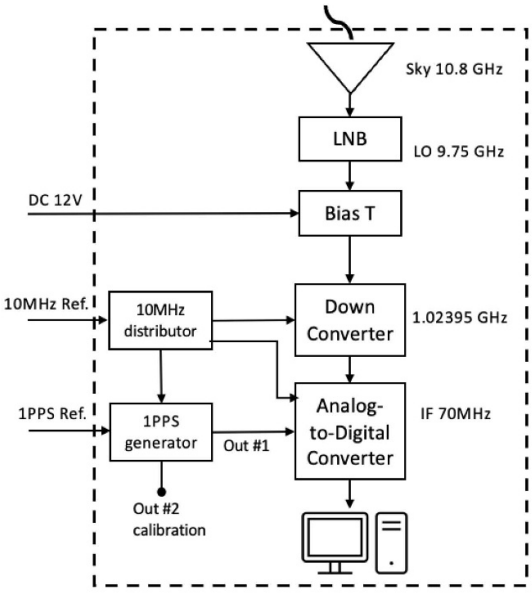
In accordance with equation (3), the calibration procedure relies on three key elements. First, the absolute position of the user antenna determined via GNSS with sub-metre accuracy. Second, the internal reference delay between the user clock and the SDR time base is measured using a TIC and a pivot technique, in which both time bases are compared against a common pivot reference so that the counter and cabling delays cancel in the difference [18]. Third, the satellite ephemeris obtained from the OD solution is interpolated at the user observation epochs to compute the signal time of flight.

Because the offsets between UTC(IT) and the other UTC(k) realisations are known from active TW measurements, this approach enables relative calibration—and thus time transfer—with respect to all UTC(k) laboratories in the network by accounting for the corresponding clock differences. The resulting calibration values are reported in table 1; to assess robustness against equipment relocation, a closure sequence was performed by repeating the calibration before and after the remote deployment to Côte d'Azur Observatory (OCA) (section 4.3).

IT01, whose composite delay is fixed in the OD, closes to 0.6 ns; as its hardware delay is unchanged between the two periods, this residual directly measures the OD ephemeris error. The larger SP01 (+2.7 ns) and PTB05 (+3.2 ns) closures reflect two compounding effects: first, unlike IT01 being anchored in the OD, these links absorb the ephemeris error in the directions poorly constrained out of the IT01 line of sight; second, the active-network calibration update at MJD 60 583 introducted an offset between the continental-European stations and IT01, which contributes to the increased closure values.

4.3. Time transfer at the OCA

The passive user terminal was deployed at the OCA, located on the Calern plateau. Applying equation (3) with the calibrated composite delays of table 1, the clock offset between UTC(OCA), acting as the passive



(a)



(b)

Figure 8. The portable passive TW user terminal. (a) Block diagram of the receive terminal and timing-reference distribution used for signal acquisition and delay calibration. (b) The 100 cm Ku-band dish antenna during deployment at the Côte d'Azur Observatory (Calern plateau).

Table 1. Calibrated passive-user composite transmission delay measured at INRiM, forming the calibration-closure sequence. The pre-trip period spans MJD 60 565–60 570 and the post-trip period MJD 60 662–60 695. $\Delta_{\mathrm{pre-post}}$ is the closure difference.

Tx station	Period	Mean ± std/ns	$\Delta_{\mathrm{pre-post}}$/ns
IT01	pre-trip	1389.7 ± 1.31	+0.6
	post-trip	1389.1 ± 0.82	
SP01	pre-trip	1401.2 ± 1.10	+2.7
	post-trip	1398.5 ± 0.66	
PTB05	pre-trip	3790.0 ± 1.09	+3.2
	post-trip	3786.8 ± 0.66	

user clock, and each UTC(k) realisation is obtained. The resulting time transfer series and their stability are shown in figure 9.

During the 40 d campaign, occasional loss-of-lock events were observed, primarily due to frequency drift of the LNB local oscillator driven by ambient temperature variations. Future deployments could mitigate this limitation through the use of temperature-stabilised or reference-locked LNBs, as well as improved SDR re-acquisition strategies such as wider initial frequency searches or predictive acquisition methods.

Independent validation is provided by co-located GNSS[10] time transfer and by active TW measurements through the OCA antenna. The passive-minus-active RMS is 1.6 ns–2.9 ns and the passive-minus-GNSS RMS is 1.3 ns–1.7 ns across the three baselines. In terms of frequency stability, the overlapping Allan deviations shows passive TW reaches $\approx 10^{-14}$ at a one-day averaging time matching the performance of GNSS demonstrating that the short-term ephemeris and atmospheric mismodelling average out and no longer limit the comparison. The residual nanosecond-level discrepancies are attributed to antenna-position uncertainties and to different calibration strategies in the reception chains: the GNSS receivers are calibrated within the BIPM scheme (G1/G2), whereas the active TW link to OCA was aligned to GNSS in the absence of a dedicated BIPM campaign.

[10] Based on GPS Common-View (CGGTTS) data generated by geodetic multi-GNSS timing receivers.

4.4. Preliminary uncertainty budget

A preliminary uncertainty budget for passive TW is summarised in table 2. The two dominant contributions are the user antenna-position uncertainty—a purely geometric term that scales at 3.3 ns per metre of position error along the line of sight, and is readily

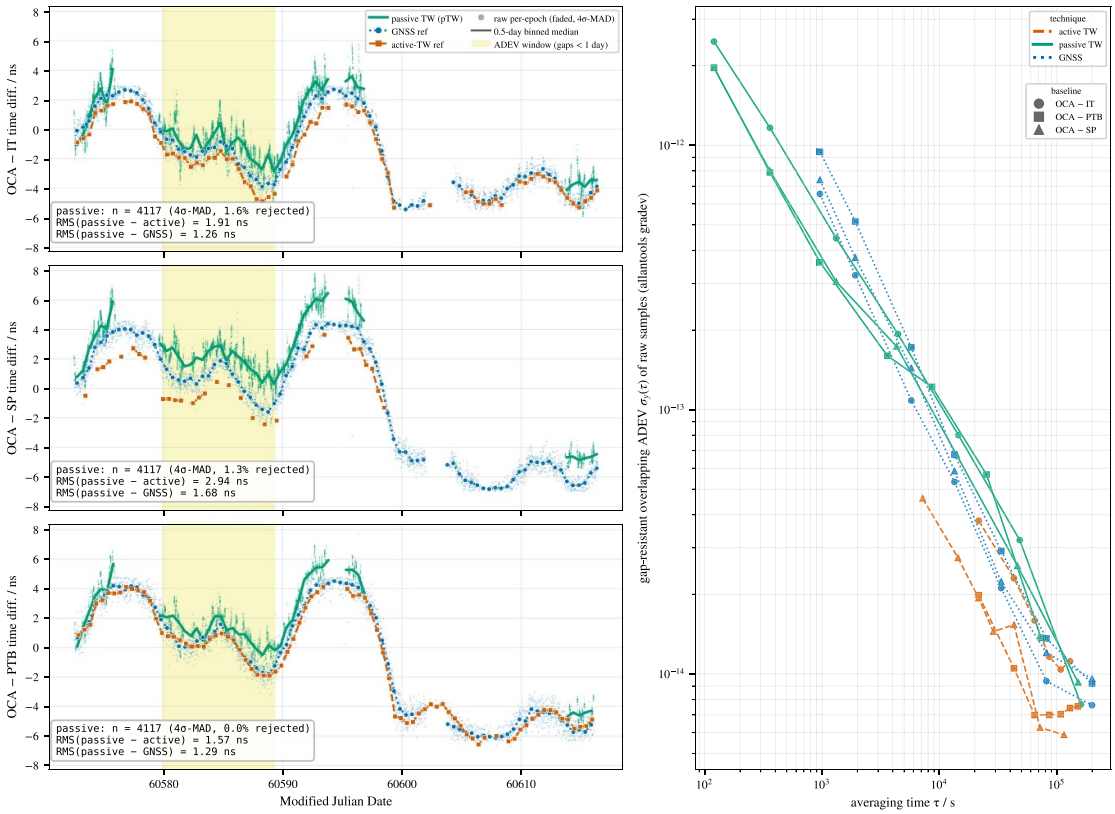


Figure 9. Passive-user OCA time transfer validated against active TW and co-located GNSS. *Left:* per-baseline time-difference series (OCA−IT, OCA−SP, OCA−PTB); faded points are the raw per-epoch values (4σ-MAD screened) and solid lines the 0.5 d binned medians, the shaded band marking the common coverage window feeding the Allan deviation. *Right:* overlapping Allan deviation $\sigma_y(\tau)$ computed on the raw per-epoch series, with line style encoding the technique and marker the baseline.

Table 2. Preliminary standard uncertainty budget (1σ) for the passive user.

Uncertainty source	Std. unc./ns	Justification
User antenna position (<1 m)	3.3	Sub-metre GNSS survey
Satellite ephemeris (short-term)	3.3	Formal error in radial direction
Residual tropospheric delay (wet)	3.0	VMF3 wet residual at low elevation
Calibration closure repeatability	3.0	EU UTC(k) pre/post-trip closure
Transponder group-delay (EU only)	1.0	Conservatively estimated from temperature variation of satellite
User terminal delay	1.0	Conservatively estimated from temperature variation of user terminal
Measurement noise	1.0	OD post-fit residual RMS
Total (RSS)	≈ 7	

reduced with a more precise survey—and the residual wet-tropospheric delay, conservatively bounded at ∼3 ns given the low satellite elevation. The short-term satellite-ephemeris error and the calibration-closure repeatability each contribute at a comparable ∼3 ns level, while the transponder and user-terminal group-delay variations and the measurement noise each contribute at the 1 ns level. Future campaigns will refine this budget using longer datasets and station loop-delay measurements at multiple sites.

It should be noted that all results presented here are obtained in post-processing, and that the passive observables are processed only *within* the manoeuvre-free estimation arcs, so the service is available ≈90% of the time. Within an arc the time transfer is consistent at the level reported above, whereas extrapolating an ephemeris through an unmodelled repositioning manoeuvre would incur errors of several tens of nanoseconds. This also indicates the mitigation strategy for quasi-real-time operation: a sustained increase in post-fit residuals flags a manoeuvre, triggering reinitialisation of the OD filter and re-estimation of the satellite state once the manoeuvre is completed (typically within one hour). If the OD process is executed routinely at the end of each active TW session (every two hours) and the updated ephemerides are distributed to passive users, the time transfer accuracy demonstrated here can be achieved with a latency of approximately three hours.

5. Conclusion and future work

This study demonstrates the end-to-end implementation of passive TW, enabling receive-only users to synchronise to UTC(k) at the nanosecond level using low-cost hardware and satellite ephemeris derived from active TW datasets. The OD approach, anchored to the single directly measured IT01 delay, enables calibration of the user receive delay in a common-clock configuration.

The method was validated over a 40 d deployment at the OCA, where passive TW agreed with both GNSS and active TW at the nanosecond level across several UTC(k) baselines. Crucially, the passive Allan deviation converges to $\approx 10^{-14}$ at one day—comparable to the GNSS—as the orbit-side errors average out; the accuracy is bounded by an ≈ 7 ns (1σ) budget. A closure sequence at INRiM confirmed robustness to relocation and traceability to UTC(k). The short-term variability is driven mainly by solar-radiation-pressure mismodelling— limited by the poorly known attitude—and wet tropospheric delay.

Future work will focus on transitioning passive TW from post-processed demonstrations to operational deployment. Key developments include automation of the OD workflow with built-in manoeuvre detection and state re-initialisation, assessment of ephemeris-extrapolation errors for quasi-real-time operation. On the terminal side, a temperature-stabilised or reference-locked LNB would mitigate the loss-of-lock events observed in the field.

From a network perspective, routine measurement and reporting of transmit and receive station delays within the active TW infrastructure would improve OD robustness and reduce systematic uncertainties. Longer-term experimental campaigns will enable a more rigorous statistical uncertainty budget. Together, these developments would position passive TW as a scalable, interference-resilient complement to GNSS for UTC(k) dissemination, particularly for applications requiring independent, traceable and secure time transfer.

Acknowledgments

The authors would like to extend their gratitude to Clément Courde and the team at the Côte d”Azur Observatory for hosting the experiment, as well as the UTC(k) labs for access to the TW datasets.

Data availability statement

The TW measurement data were provided by the participating UTC(k) laboratories under data-sharing agreements and are not publicly available. Processed results are available from the corresponding author upon reasonable request. The Tudat astrodynamics software used for orbit determination is openly available at: https://docs.tudat.space/en/latest/.

Funding

This work was supported by INRiM, and performed as part of Michael Plumaris”s PhD at Sapienza University of Rome.

Author contributions:

M. Plumaris: Methodology, Software, Data Analysis, Visualization, Writing T. Thai: Investigation, Validation D. Rovera: Conceptualization, Validation L. Iess: Supervision –Review–Editing. D.Dirkx: Software–Review–Editing. I. Sesia: Conceptualization, Supervision, Project Administration

ORCID iDs

Michael Plumaris 0000-0003-3260-9438
Tung Thai 0000-0002-1750-0998
Daniele Rovera 0000-0003-1539-4965
Luciano Iess 0000-0002-6230-5825
Dominic Dirkx 0000-0003-2069-0603
Ilaria Sesia 0000-0002-3309-6737

References

[1] Hanson D W 1989 Fundamentals of two-way time transfers by satellite *Proc. 43rd Annual Symp. on Frequency Control* pp 174–8
[2] Kirchner D 1991 Two-way time transfer via communication satellites *Proc. IEEE* **79** 983–90
[3] ITU Radiocommunication Sector 2015 *The Operational use of two-way Satellite Time and Frequency Transfer Employing Pseudorandom Noise Codes. (Recommendation itu-r Tf.1153-4)* (International Telecommunication Union)
[4] Rieck C, Jarlemark P and Jaldehag K 2018 Passive utilization of the TWSTFT technique *European Frequency and Time Forum (EFTF)* (IEEE) pp 263–9
[5] Tavella P *et al* 2016 Time dissemination services: Experimental results of the european H2020 DEMETRA project *IEEE Int. Frequency Control Symp. (IFCS)* pp 1–5
[6] T Telstar 2008 11n technical manual *Tech. Rep.* Telesat
[7] Gisolfi L *et al* 2025 Open-source high-fidelity orbit estimation for planetary science and space situational awareness using the Tudat software
[8] Dirkx D *et al* 2022 The open-source astrodynamics TudatPy software: overview for planetary mission design and science analysis *Europlanet Science Congress 2022* (*Palacio de Congresos de Granada, Spain, 18–23 September 2022*) pp 2022–253
[9] Corey R L and Pidgeon D J 2009 Electric propulsion at space systems/loral *Int. Electric Propulsion Conf.*
[10] Skipper J K, Racicot D, Li S, Provencher R and Palimaka J 2004 Hybrid (ion and chemical) GEO stationkeeping maneuver planning software *SpaceOps Conf.* p 499

[11] Landskron D and Böhm J 2018 VMF3/GPT3: Refined discrete and empirical troposphere mapping functions *J. Geod.* **92** 349–60
[12] Server V M F D 2020 Registry of research data repositories
[13] Iess L, Di Benedetto M, James N, Mercolino M, Simone L and Tortora P 2014 ASTRA: Interdisciplinary study on enhancement of the end-to-end accuracy for spacecraft tracking techniques *Acta Astronaut.* **94** 699–707
[14] Jakowski N, Hoque M M and Mayer C 2011 A new global TEC model for estimating transionospheric radio wave propagation errors *J. Geod.* **85** 965–74
[15] Ashby N 2003 Relativity in the global positioning system *Living Rev. Relativ.* **6** 1
[16] Hauschild A 2017 Basic observation equations *Springer Handbook of Global Navigation Satellite Systems* (Springer) pp 561–82
[17] Jiang Z *et al* 2018 Use of software-defined radio receivers in two-way satellite time and frequency transfers for UTC computation *Metrologia* **55** 685
[18] Rovera G D, Siccardi M, Römisch S and Abgrall M 2019 Time delay measurements: Estimation of the error budget *Metrologia* **56** 035004